frontiers | Frontiers in Earth Science

TYPE Original Research
PUBLISHED 23 February 2023
DOI 10.3389/feart.2023.1144283

OPEN ACCESS

EDITED BY
Jia-Wen Zhou,
Sichuan University, China

REVIEWED BY
Huei-Fen Chen,
National Taiwan Ocean University, Taiwan
Shengli Yang,
Lanzhou University, China

*CORRESPONDENCE
Yuzhu Zhang,
xbdzyz05@nwu.edu.cn

SPECIALTY SECTION
This article was submitted to Quaternary Science, Geomorphology and Paleoenvironment, a section of the journal Frontiers in Earth Science

RECEIVED 14 January 2023
ACCEPTED 13 February 2023
PUBLISHED 23 February 2023

CITATION
Wang S, Wang N, Zhang Y, Huang C, Zhu Y, Xiao Q, Chen D, Wang H, Ming Y, Huang X and Wang S (2023), Geochemistry of a paleo-oxbow lake sediments and its implications for the late Holocene extreme overbank flooding history of the Yellow River within the Zoige Basin, NE Tibetan Plateau. *Front. Earth Sci.* 11:1144283. doi: 10.3389/feart.2023.1144283

Geochemistry of a paleo-oxbow lake sediments and its implications for the late Holocene extreme overbank flooding history of the Yellow River within the Zoige Basin, NE Tibetan Plateau

Shuo Wang[1], Ninglian Wang[1,2], Yuzhu Zhang[1,3]*, Chang Huang[1], Yan Zhu[1], Qili Xiao[1], Dou Chen[1], Haoyu Wang[1], Yisen Ming[1], Xiaoling Huang[1] and Sikai Wang[1]

[1]Shaanxi Key laboratory of Earth Surface System and Environmental Carrying Capacity, College of Urban and Environmental Science, Northwest University, Xi'an, China, [2]CAS Center for Excellence in Tibetan Plateau Earth Sciences, Beijing, China, [3]State Key Laboratory of Loess and Quaternary Geology, Institute of Earth Environment, Chinese Academy of Sciences, Xi'an, China

Paleo-oxbow lake sediments can provide archives to reconstruct paleo-channel evolution and flooding history of the river. Multi-proxy approaches including detailed sediment stratigraphy, sedimentology and geochemistry have been implemented in a high-resolution sedimentary section of paleo-oxbow lake of the Yellow River within the Zoige Basin on the NE Tibetan Plateau, to reconstruct regional environmental changes and extreme overbank flooding history. Our results suggest that not only traditional sedimentological proxies, but also chemical elements can be applied in defining sequences with different genetic types, especially the paleoflood deposits in the paleo-oxbow profile. Two units of late-Holocence extreme overbank flooding deposits (OFDs) are identified in terms of the significantly higher proportions of sand, high contents of SiO_2, Na_2O, Ba, low contents of Al_2O_3, Fe_2O_3, MgO, K_2O, Ti, Rb and high values of Zr/Fe, Zr/Rb ratios. These extraordinary flood events within the Zoige Basin were dated back to 2,960 ± 240–2,870 ± 270 a and 1840 ± 200–1700 ± 160 a, in response to the mid-Holocene climatic optimum to the late Holocene and the Dark Age Cold Period (DACP). And the strong rainfall caused by the abnormal atmospheric circulation during the period of climate transition and abrupt change may led to the frequent occurrence of extreme flood events in the source region of the Yellow River. These findings are important for understanding the response of regional fluvial system to high climatic instability and provide a new perspective for us to analyze the risk of flood disasters on the Tibetan Plateau under the background of climate change.

KEYWORDS

Yellow River, Tibetan Plateau (TP), oxbow lake, paleoflood, climatic variability

1 Introduction

It is generally accepted that lakes are highly sensitive to environmental change and its response to the major climate fluctuations is extremely complex (Woolway and Merchant, 2019; Zhang et al., 2020). Oxbow lakes, as a special type of abandoned channels formed by curve cut-off of meandering rivers in the alluvial plain, play an important role in describing relationships between environmental change and the fluvial dynamics of the systems (Pawłowski et al., 2015). Sediment delivery and deposition at low energy locations result in the accumulation of organic matter, silt, and clay, and these undisturbed sediment fines preserve the sedimentation and geochemical record in the oxbow lake watershed (Bábek et al., 2011; Petr et al., 2013). In recent years, the multi-proxy approaches including pollen analyses, radiocarbon dating, detailed sediment stratigraphy, micromorphology and geochemistry, have been implemented in high-resolution lacustrine deposits of oxbow lakes to reconstruct paleohydrological environment and track past climatic change (Xiao et al., 2022; Antczak-Orlewska et al., 2021; Galicki et al., 2018; Petr et al., 2013).

The element geochemistry has been used as an indicator of past climatic and environmental changes across a wide range of timescales (Wennrich et al., 2014; Arnaud et al., 2016; Francke et al., 2020). For example, Rb/Sr ratios have been widely applied to reflect chemical weathering intensity and climate change on geological timescales (Chen et al., 1999a; Fritz et al., 2018; Yang et al., 2020). The chemical index of alteration (CIA) were used as a paleoclimatic indicator to reconstruct weathering process and pedogenesis as well as the intensity of the East Asian summer monsoon and westerlies (Goldberg and Humayun, 2010; Jia et al., 2022). The elemental distribution (such as Al, Fe, K, Mg, Mn, Ca, and Na) of river and lake sediment have important tracing significance on studies about the regional features of the catchment, the transformation of soils, and the hydrogeological conditions (Brown, 2011; Vogel et al., 2015; Hasberg et al., 2019).

The northeastern (NE) Tibetan Plateau is affected by the Prevailing westerlies (PW), East Asian summer monsoon (EASM) and Indian summer monsoon (ISM), which is a sensitive area in response to global climate change (An et al., 2012; Chen et al., 2016; Li et al., 2019). Channel migration of the Yellow River and its tributaries have left countless meander scars, abandoned channels, and (paleo-) oxbow lakes across the Zoige Basin on the NE Tibetan Plateau, after the demise of the Zoige paleo-lake in the last stage of the late Pleistocene (Huang, 2021). These (paleo-) oxbow lakes experienced the transition from distant river sediment input to the nearby lake sediment, providing the valuable archives to document the entire basin's evolution during the late Pleistocene and Holocene. However, previous researches of the (paleo-) oxbow lakes within the basin were mainly on the channel stability and ecological effects rather than its indicative significance of paleo-environmental changes (Li and Gao, 2019; Zhou et al., 2019; Wang et al., 2020; Guo et al., 2021).

Oxbow lake deposits may also include a continuous record of flood events and are appropriate to reconstruct the flooding history of a river over time intervals of several millennia (Wolfe et al., 2006; Berner et al., 2012; Munoz et al., 2018; Fuller et al., 2019; Toonen et al., 2020). Under the influence of the river system, oxbow lake sedimentation is primarily dominated by local flooding, backwater flooding, overland river flow, and tributary runoff (Galicki et al., 2018). High energy discharge during floods can result in an increase in coarse-grained material and is accompanied with significant changes in chemical-mineralogical contents in oxbow lake sediments (Wolfe et al., 2006; Berner et al., 2012). Predicted climate warming is likely to change future flood magnitude and frequency as the hydrological cycle intensifies in the headwater region on the Tibetan Plateau (Lutz et al., 2016; Wang et al., 2016; Gu et al., 2018). Hence, there is a need to better understand relationships between climatic changes and extreme flood event variability and requires paleoflood reconstruction to improve our ability to assess the risk of low-frequency, high-magnitude flood events (Baker, 1987; Wilhelm et al., 2018). This paper presents our new paleoflood investigations in the source region of Yellow River. Based on field observations and sedimentological analysis, a representative paleo-oxbow lake fill at NYQ-B site (NYQ-B profile) within the Zoige Basin was studied. Using different geochemical characteristics in overbank flood deposits and paleo-oxbow lake deposits, combined with other lithological and sedimentological proxies, we reconstruct paleoflood activities of the Yellow River within the Zoige Basin, and demonstrate the fluvial and geomorphic response to climatic changes on the NE Tibetan Plateau during the late Holocene.

2 Geographical settings

The Zoige Basin is a Cenozoic fault depression (pull-apart basin) located on the NE Tibetan Plateau between latitudes 32°17′N and 32°7′N and longitudes 101°30′E and 103°22′E, covering an area of 19,400 km^2 (Figure 1; Wang and Xue, 1997). The majority of the area is 3,400–3,600 m a.s.l, surrounded by the Anyemaqen, Nianbaoyuze and Qionglai Mountains of elevations >4,000 m (Figure 1). These surrounding mountains are annually snow-covered and have paleo-glacier relics. The basin is affected by PW, EASM and ISM, which is a sensitive area in response to global climate change (An et al., 2012; Chen et al., 2016; Li and Gao, 2019). The annual average temperature ranges from 0.6°C to 1.2 °C (the minimum and maximum monthly temperature is −9.0°C in January and 11.5°C in July, respectively). The mean annual precipitation ranges from 600 to 700 mm and monthly precipitation is mainly concentrated between May and October, accounting for 90% of the annual total (610 mm) (Hu et al., 2018).

The Zoige Basin is characterized by wide river valleys and lakes are distributed among low hills. The main rivers within the Zoige Basin include the Yellow River and its tributaries such as the White River, the Black River, and the Jiaqu River. The Yellow River flows southeast into the basin about 110 km, turns northwest at the intersection with the White River and flows out after receiving the Black River, which forms a huge U-shaped bend known as the "First Bend of the Yellow River" (Figure 1). Along the way, variations of stream gradient and bed sand constituent make the river pattern of the Yellow River changes repeatedly, leaving more than 150 oxbow lakes within Zoige Basin (Li and Gao, 2019; Huang, 2021).

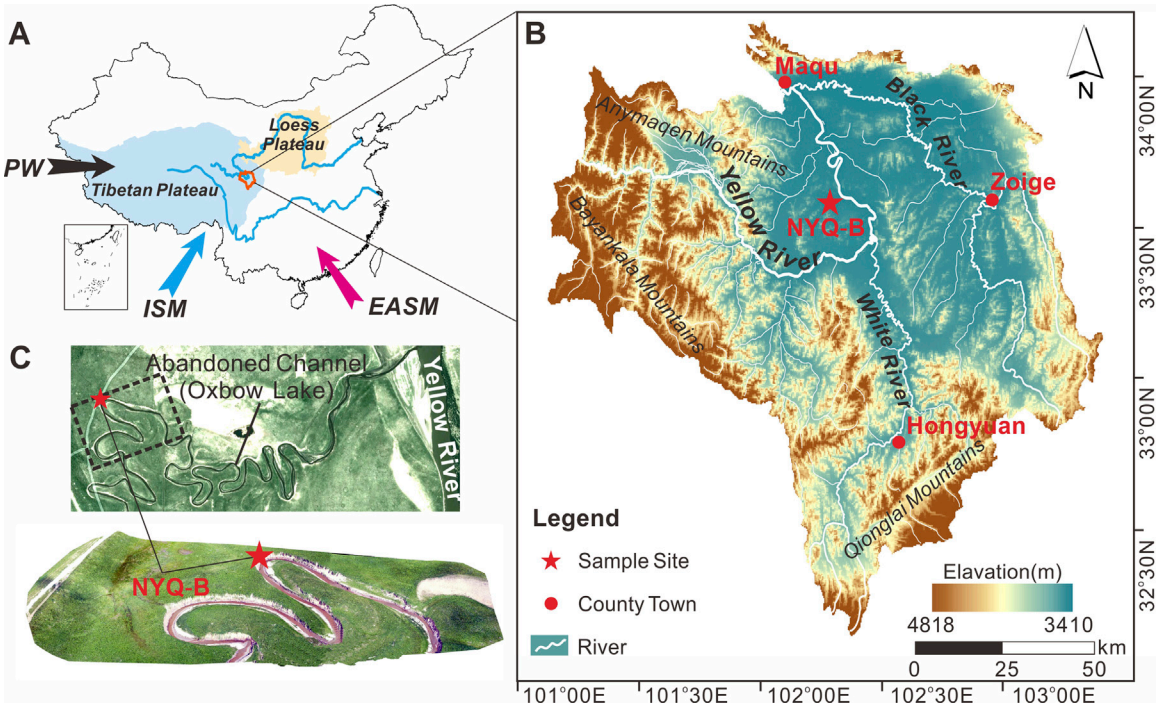

FIGURE 1
Overview of the study area. **(A)** Map shows the Zoige Basin (the outlined area) on the NE Tibetan Plateau; Abbreviation: PW, Prevailing Westerlies; ISM, Indian summer Monsoon; EASM, East Asian summer Monsoon. **(B)** Geomorphology of the Zoige Basin and the location of the paleo-oxbow lake fill at NYQ-B site in the Yellow River within the Zoige Basin. **(C)** The satellite image (Google Earth) and our UAV aerial image shows the location of the paleo-oxbow lake fill at NYQ-B site in the Yellow River within the Zoige Basin.

3 Materials and methods

3.1 Fieldwork

A detailed geological survey showed that a large number of paleo-oxbow lakes formed along the huge U-shaped bend of the Yellow River within the Zoige Basin on the NE Tibetan Plateau. The paleo-oxbow lake fill at the NYQ-B site (33°37′12″N, 102°18′44″E) in the Yellow River within the basin was studied (Figure 1C). The NYQ-B profile is situated in a Ω-shaped paleochannel at the back edge of the first river terrace (T_1) and 5 m above the present normal water level of the Yellow River. As the paleochannel is deeply cut by the Niangyiqu branch, the profile is freshly exposed and has clear stratigraphic boundaries (Figure 2). Detailed filed observation and stratigraphic description (color, structure and texture) were made in the field (Table 1).

3.2 Geochemical and sedimentological analysis

Chemical composition was determined in 69 samples taken every 5 cm, using a Bruker S2 RANGER Energy Dispersive X-Ray fluorescence spectrometer. 4 g of dried and homogenized sediments were put into the mold and smoothed, using boric acid base to edge. Then the sample was put into the press machine (30 t pressure) and pressed into circular sheets for measurements. Precision and accuracy of the chemical analysis for major (K, Ca, Na, Mg, Al, Fe, Si) and trace elements (Co, Zr, Rb, Sr, Ti, Zn, Cu, Pb, Ba, Cr, Mn, As, P, S) was checked by repeated measurements of the certified reference material including a Cu disk and a glass BAXS-S2 with the determination error <5%. For a typical analyses process and the precision of all elements refer to Shehata Ahmed Hussein (2016). Magnetic susceptibility was measured on a mass of 10 g of sediment with a Bartington MS-2B magnetic susceptibility meter (0.47/4.7 kHz). Grain-size distribution was measured by a Backman Coulter LS13320 laser analyzer with $(NaPO_3)_6$ as a dispersing agent after pre-treatment with 30% H_2O_2 (to remove organic matter) and 10% HCl (to remove carbonates), respectively.

3.3 Principal component analysis

The principal component analysis (PCA) is used to represent the elemental dataset with a few components instead of a large number of variables, group the elemental variables and detect main influential factors of element distribution (Ringnér, 2008). In this study, the function rda in the core package of vegan in R language was used to extract the feature quantity of the element concentration data to complete the principal component analysis (Borcard et al., 2018). The functions of summary and loadings ware used to query the information of each principal component and check the contribution of each variable to the principal component. The function biplot (using scaling 1 and scaling 2, respectively) was applied to plot the samples and project the elements over the principal component, visualizing

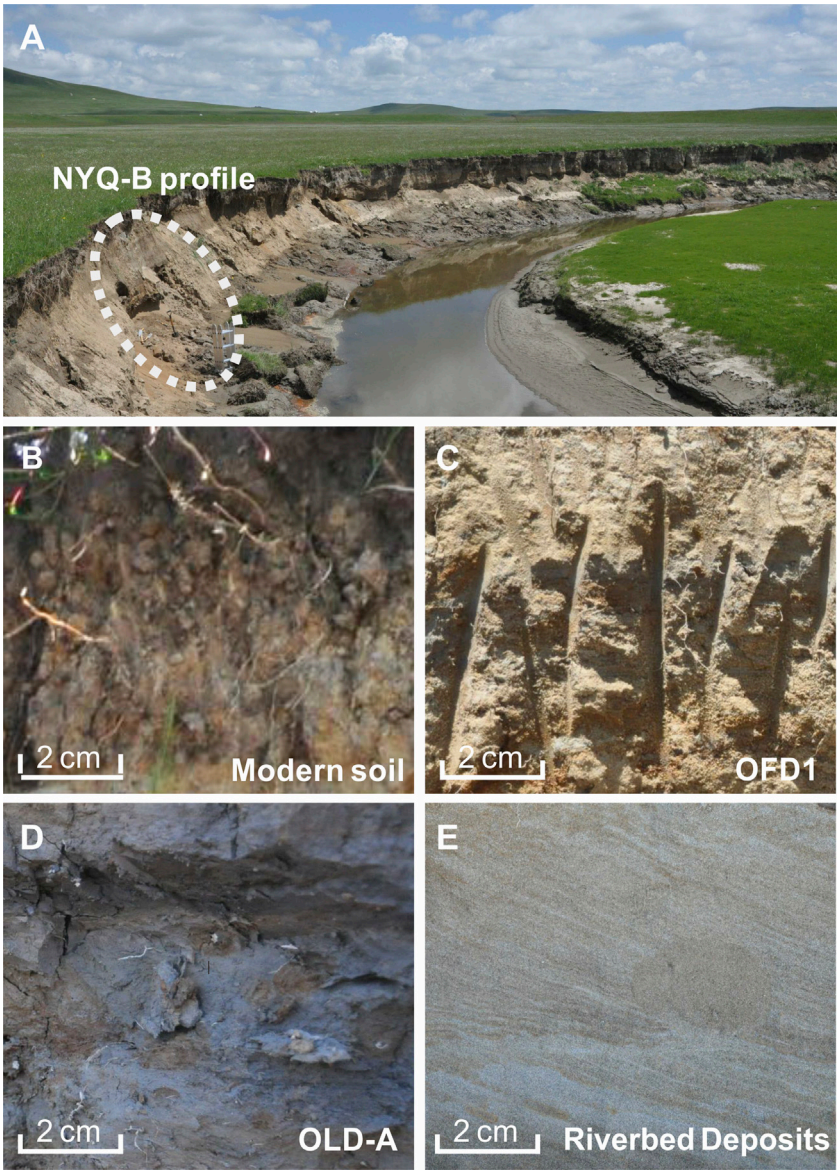

FIGURE 2
(A) Photo showing the paleo-oxbow lake fill at NYQ-B site within the Zoige Basin on the NE Tibetan Plateau. **(B–E)** Close-up shots showing difference between modern soil, overbank flooding deposits (OFD), paleo-oxbow lake deposits (OLD) and riverbed deposits (RD) at the NYQ-B site.

correlations between samples and determine whether samples can be grouped (Borcard et al., 2018). The arrow lengths of elements in distance biplot (scaling 1) showing their contribution to the principal components, and the correlation biplot (scaling 2) reveals distinct element clusters and the elements within the one cluster are highly correlated (Ter Braak, 1983; Legendre and Gallagher, 2001).

4 Results

4.1 Stratigraphy and chronology

In the NYQ-B profile within the Zoige Basin on the NE Tibetan Plateau, the sediment sequence was divided into six units according to the lithology and sedimentary structures from the base upwards (Figure 3). The unit of riverbed deposits consisting of fine sand and medium sand with parallel beddings were clearly visible at the bottom (340–215 cm). And two units of the paleo-oxbow lake deposits (OLD-A and OLD-B) were found in the depth range of 215–200 cm and 170–80 cm, which were composed of brown black clayey silt, with a hard texture and rich in organic matter. Two units of overbank flood deposits (OFD1, OFD2) with parallel and wavy beddings were also identified at 200–170 cm and 80–35 cm, respectively. The OFD2 unit was split into three sublayers, OFD2-1, OFD2-2 and OFD2-3, indicating that several episodes of overbank flooding occurred during the late Holocene (Huang et al., 2011a; 2011b; 2010; Xiao et al., 2022). The layer of typical subalpine meadow

TABLE 1 Pedosedimentary descriptions of the paleo-oxbow lake fill at NYQ-B site within the Zoige Basin on the NE Tibetan Plateau.

Depth (cm)	Pedostratigraphic subdivisions	Pedosedimentary descriptions
35–0	Modern soil (MS)	Gray, clayey silt, granular-block structure, loose and porous, some earthworm burrows and excrement, well-developed plant roots.
50–35	Overbank flood deposits (OFD2-3)	Yellowish orange, silty fine sand, some rust spots, very loose.
68–50	Overbank flood deposits (OFD2-2)	Grayish-white, silty fine sand, some rust spots, very loose.
80–68	Overbank flood deposits (OFD2-1)	Yellowish orange, silty fine sand, some rust spots, unconformable contact with the underlying oxbow lacustrine deposits.
80–170	Paleo-oxbow lake deposits (OLD-B)	Brown, interbedding of clayey silt and fine sandy silt, some rust spots, relatively firm.
200–170	Overbank flood deposits (OFD1)	Yellowish orange, medium sandy fine sand, some rust spots, very loose, some parallel or waving beddings.
215–200	Paleo-oxbow lake deposits (OLD-A)	Brown black, clayey silt, rich in organic matter, relatively firm.
340–215	Riverbed deposits (RD)	Dull yellowish orange, fine sandy medium sand, some rust spots, with inclined beddings.

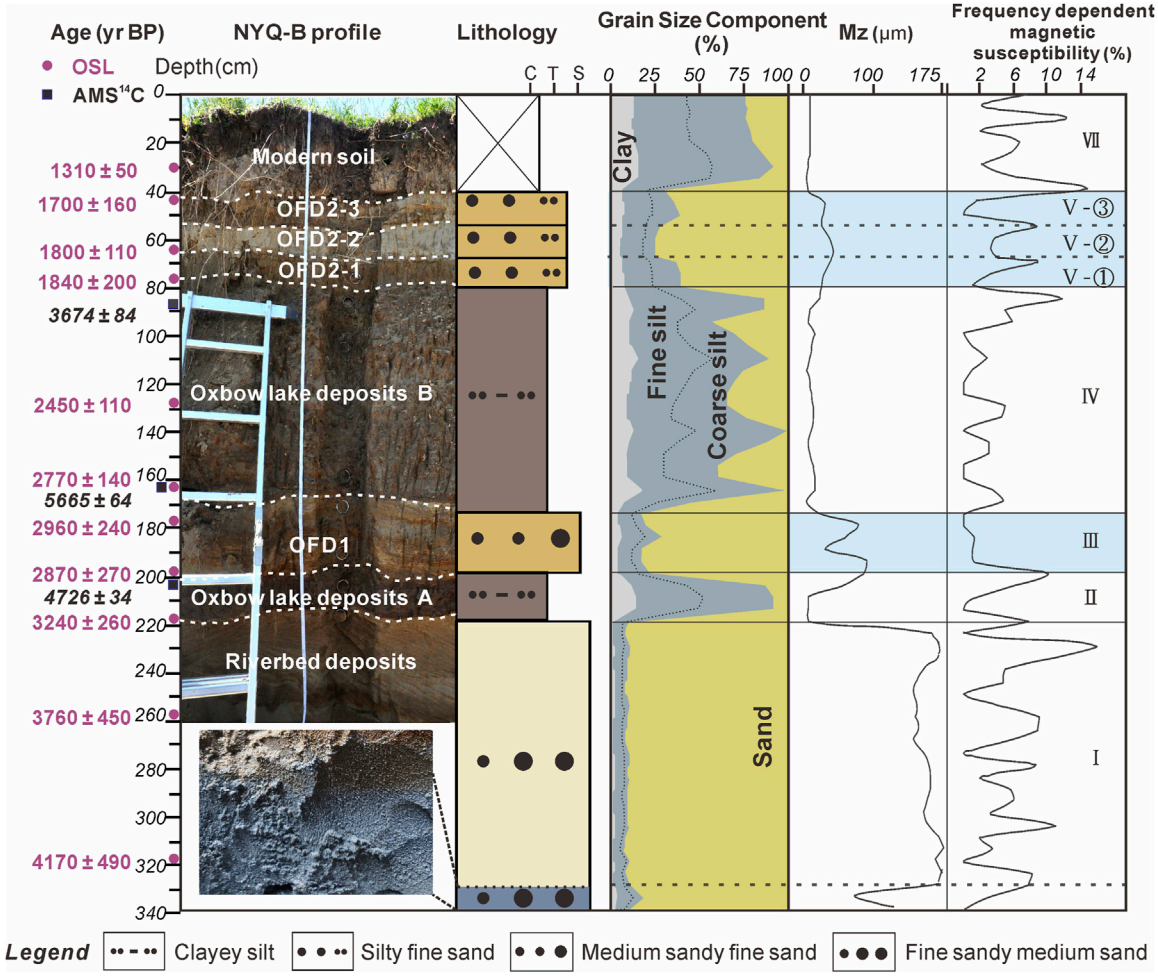

FIGURE 3
Sedimentary framework of the paleo-oxbow lake fill at NYQ-B site within the Zoige Basin on the NE Tibetan Plateau, including lithology, dating results, grain size parameters, magnetic susceptibility and frequency dependent magnetic susceptibility. The results of AMS ^{14}C and OSL dating in Figure 3 refer to Xiao et al., 2022.

soil were found at surface (35–0 cm), which comprised grey clayey silt with abundant earthworm burrows and plant roots. In particular, the chronology of the NYQ-B profile was dated by using the AMS ^{14}C and OSL dating techniques (Xiao et al., 2022) (Figure 3). However, the AMS ^{14}C ages are inverted and obviously older than OSL ages as a result of the re-working of old carbon during the paleo-oxbow lake depositional process (Zhou et al., 2016; Kołaczek et al., 2017). And then, these AMS ^{14}C ages were dropped. In summary, the dating results showed that two episode of extraordinary overbank flooding recorded by the OFDs occurred at 2,960 ± 240 to 2,870 ± 270 a and 1840 ± 200 to 1700 ± 160 a, respectively (Xiao et al., 2022).

4.2 Grain-size distribution and magnetic susceptibility

The grain-size distribution in the NYQ-B profile within the Zoige Basin is shown in Figure 3. The clay (<2 μm), fine silt (2–16 μm), coarse silt (16–63 μm), and sand (>63 μm) ratio vary considerably in the six units of the profile NYQ-B. The significant low values of the mean grain size show in the paleo-oxbow lake deposits (OLD-A and OLD-B), while high values in the overbank flood deposits (OFD1 and OFD2) and riverbed deposits.

Unit I (from the bottom to 215 cm) is composed of riverbed deposits, therefore, the sediment is the coarsest and dominated by sand (90.2%), with a little bit of silt (7.6%) and clay (2.2%). The sediment of Unit II (215–200 cm, OLD-A) is the finest and the sand component sharply reduces to 8.2%, while the silt component reaches its highest levels of the profile (76.8%) and clay content is 15.0% Unit III (200–170 cm, OFD1) is dominated by sand content again (79.2%), while silt content decreases to 16.0% and clay content falls further to 4.8% In Unit IV (170–80 cm, OLD-B), Mean silt content increases to 63.7% on average and sand reduces to 24.8% (Figure 3). It is noteworthy that sand content has been reduced to <1% at some depths. There is also substantial variation here in mean particle size, from 8.5 to 41.6 μm, with a mean value of 20.8 μm. Unit V (80–35 cm, OFD2) is divided into three sections, OFD2-1, OFD2-2 and OFD2-3 according to the mean particle size. Mean particle size of OFD2-2 (72.2 μm) is much coarser than the OFD2-1 and OFD2-3 (51.2 and 50.5 μm, respectively), and the sand content of OFD2-2 further increased to 74.3% than 60.4% and 65.0% in the OFD2-1 and OFD2-2. Unit VI (35–0 cm) is dominated by silt again (68.0%) with clay (13.8%) and sand (18.2%). Mean grain size also decrease to 9.9–18.3 μm.

In water-laid deposits, the frequency magnetic susceptibility reflects predominantly the supply of exogenic very fine-grained material, which means clay minerals deposited from suspension (Petr et al., 2013). Grain-size and Magnetic susceptibility data have been reported in previous papers (Xiao et al., 2022), but the frequency dependent magnetic susceptibility (χ_{fd}) is calculated in this study (Figure 3), to indicate the concentration of ferromagnetic minerals in the sediments and distinguish between the flooding units and the paleo-oxbow lake deposits combined with grain size distribution. The units with high frequency dependent susceptibility (χ_{fd}) have a finer average grain size. For example, the average χ_{fd} of surface layer (modern soil) is 6.61%, and the highest reach to 14.8%; the average χ_{fd} value of the OLD-A is 5.01% with the maximum value of 10.2% and the layer of the OLD-B has the maximum value of 11.7%. It means that magnetic minerals in sediments are composed of a relatively high proportion of super fine particles (superparamagnetic/single-domain threshold) which only contribute to the low-frequency susceptibility (Zhou et al., 1990; Liu et al., 2005). In contrast, the χ_{fd} of OFD1, OFD2 layers are lower than those of the pale-oxbow lake deposits, with the mean values of 0.70%, 3.82%; the highest value of OFD1, OFD2 layers are 1.3%, 8.9% and the lowest value is close to 0. And the χ_{fd} value of riverbed deposits fluctuates greatly and the average value is 5.11%. We infer that extreme hydrodynamic force during flood events brought more coarse terrigenous material into the paleo-oxbow lake fill at NYQ-B site, leading to a decrease in the contribution of superparamagnetic particles to magnetic susceptibility and a very low frequency magnetic susceptibility (Wu, 1993).

4.3 Element geochemistry

The variation of representative major element oxides and trace elements and their ratios can be roughly divided into 6 units from bottom to top (Figures 4, 5).

Unit I (340–215 cm, RD): The element content in this unit shows little fluctuation (Figures 4, 5). The average content of SiO_2 is the maximum of the whole section; while the mean values of Al_2O_3, Fe_2O_3, CaO, K_2O, MgO, Ti, P, S, Zr, Rb, Sr, Zn, Cu are the minimum of the whole section (Table 2; Figures 4, 5). The average contents of Ba, Cr are as the maximum values in all sedimentary units. The average Zr/Rb, Cu/Zn ratios are the minimum of the whole section and the average Zr/Fe ratio is as a comparatively small value (Table 2; Figure 5).

Unit II (215–200 cm, OLD-A): The element content in this unit appears change suddenly compared with those in Unit I. The average content of SiO_2 is a comparatively small value of the whole section (Table 2; Figure 4). The mean values of Al_2O_3, K_2O, MgO, Ti, Mn, Zr, Rb, Zn, Cu increase to the maximum of the whole section, the contents of Ba, Cr, Na_2O significantly decrease and CaO, Sr change little. The average Zr/Fe, Zr/Rb and Cu/Zn ratios are higher than those of the Unit I (Table 2; Figures 4, 5).

Unit III (200–170 cm, OFD1): The distribution of element content in this unit is obviously different from that in the previous unit. The SiO_2, Na_2O, Ba, Cr contents increase sharply to relatively large values in the whole section. The mean values of Al_2O_3, Fe_2O_3, K_2O, MgO, Ti, Mn, P, S, Zr, Zn, Cu and Rb drop significantly. The content of CaO increases and the content of Sr decreases slightly. The average Zr/Rb, Cu/Zn ratios decrease and the Zr/Fe ratio keeps as 0.007 (Table 2; Figures 4, 5).

Unit IV (170–80 cm, OLD-B): The element contents in this unit are similar to those in Unit II but fluctuate markedly (Figures 4, 5). The average content of SiO_2 drops dramatically to the minimum of the whole section and the Na_2O, Ba, Cr contents also decrease sharply. The mean values of Al_2O_3, Fe_2O_3, K_2O, MgO, Ti, Mn, P, S, Zr, Rb, Zn, Cu increase significantly. The average contents of CaO and Sr increase sharply to the highest value (Table 2; Figures 4, 5). The Zr/Fe ratio decreases to the minimum with the value of 0.005. The average Cu/Zn ratio increases to the maximum value of 0.36 in the whole section (Table 2; Figures 4, 5).

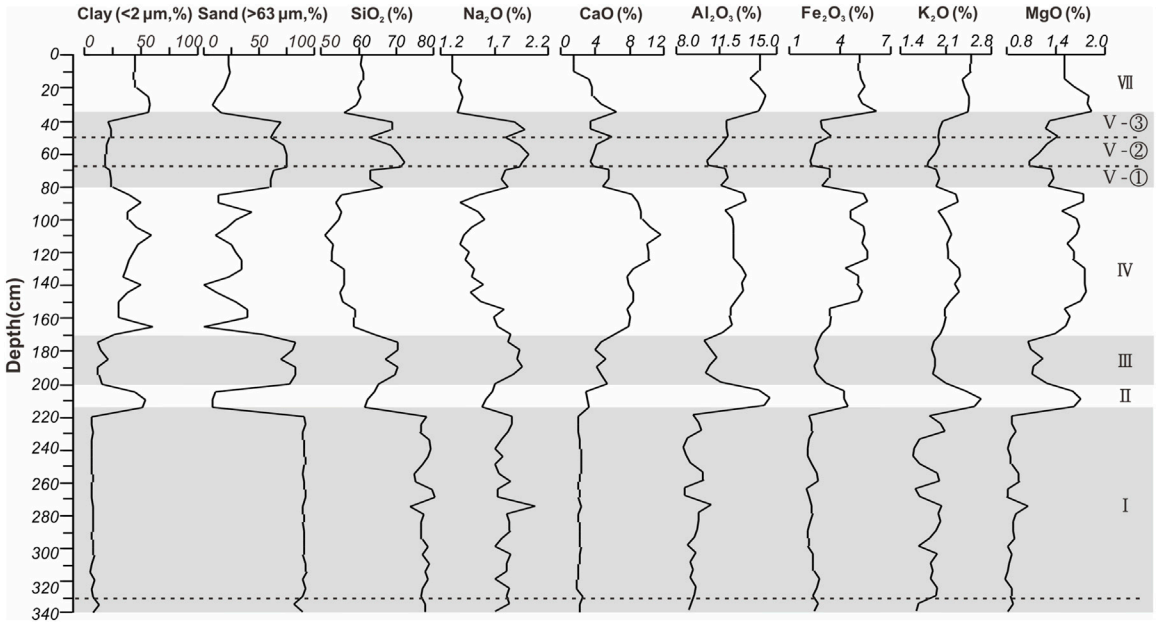

FIGURE 4
Grain size distribution and major element SiO_2, Na_2O, CaO, Al_2O_3, Fe_2O_3, K_2O, and MgO concentrations of the paleo-oxbow lake fill at NYQ-B site within the Zoige Basin on the NE Tibetan Plateau.

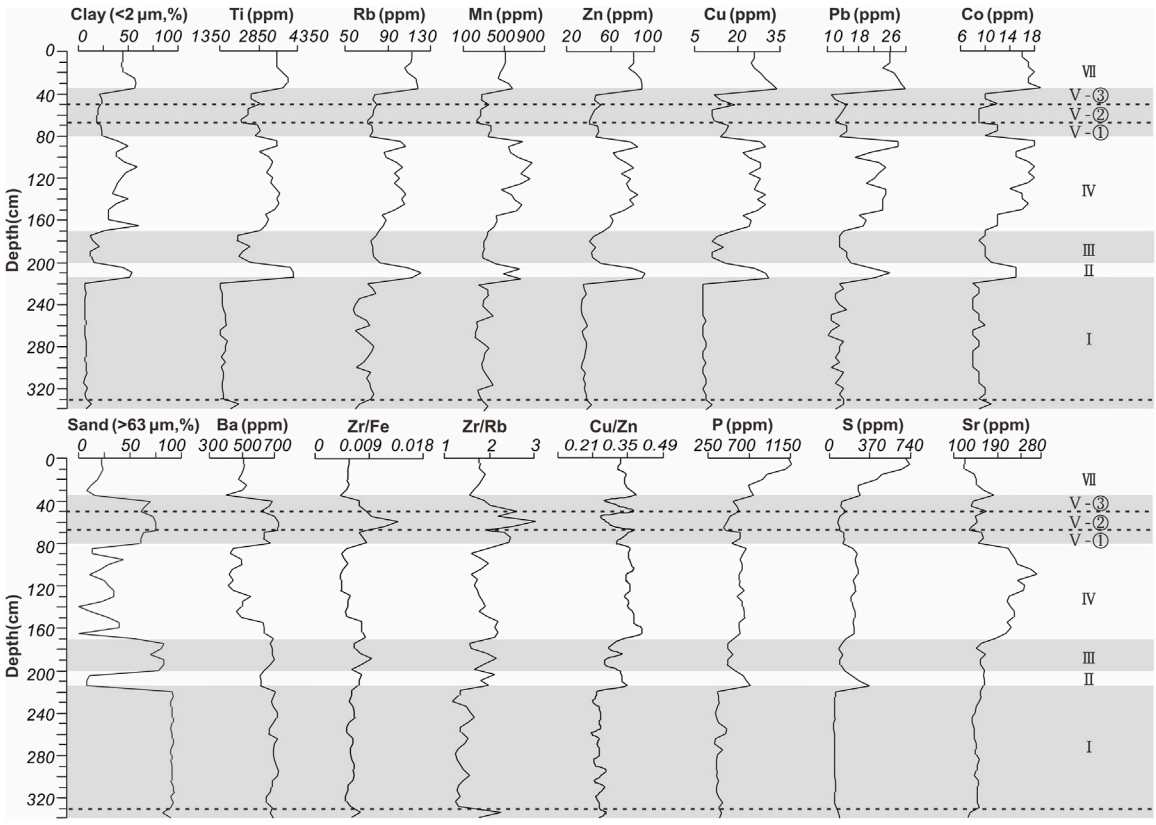

FIGURE 5
Grain size distribution and trace element Ti, Rb, Mn, Zn, Cu, Pb, Co, Ba, P, S, Sr concentrations and element ratios of Zr/Fe, Zr/Rb, and Cu/Zn of the paleo-oxbow lake fill at NYQ-B site within the Zoige Basin on the NE Tibetan Plateau.

TABLE 2 Average content of major elements oxides, trace elements and element ratios of the paleo-oxbow lake fill at NYQ-B site within the Zoige Basin on the NE Tibetan Plateau.

Elements	Modern soil	Riverbed deposits	Oxbow lacustrine deposits		Overbank flood deposits			
			OLD-A	OLD-B	OFD1	OFD2-1	OFD2-2	OFD2-3
SiO_2 (%)	59.93	77.50	62.84	55.61	69.01	64.24	70.78	66.84
Al_2O_3 (%)	13.77	9.27	14.14	12.15	10.49	11.41	10.58	11.54
Fe_2O_3 (%)	5.30	2.33	4.30	4.73	2.70	3.21	2.35	3.06
CaO (%)	3.22	2.08	3.03	8.81	4.63	5.27	3.73	4.19
K_2O (%)	2.45	1.85	2.53	2.17	1.95	1.98	1.90	2.02
Na_2O (%)	1.35	1.80	1.63	1.56	1.87	1.80	1.96	1.89
MgO (%)	1.63	0.84	1.64	1.63	1.14	1.33	1.14	1.33
Ti (ppm)	3698	1505	4151	3328	2222	2802	2297	2666
Ba (ppm)	491.63	691.24	613.00	507.67	674.67	647.00	718.75	659.33
Mn (ppm)	508.50	298.76	609.00	589.83	323.83	359.33	255.75	298.33
P (ppm)	905.38	364.96	670.00	610.61	486.00	569.33	453.25	556.67
S (ppm)	477.13	55.44	283.33	227.78	112.67	134.67	91.25	128.00
Cr (ppm)	115.63	146.04	93.33	89.89	119.50	94.33	121.50	103.33
Zr (ppm)	197.31	97.24	223.67	177.94	138.17	179.33	177.75	168.33
Rb (ppm)	112.94	69.00	114.33	96.50	77.50	74.67	73.75	78.00
Sr (ppm)	142.94	145.40	161.67	224.94	156.67	156.67	139.50	147.67
Zn (ppm)	83.50	36.20	87.00	71.94	44.33	47.67	41.75	47.33
Cu (ppm)	28.31	8.48	29.00	26.00	12.83	15.67	12.25	15.00
Pb (ppm)	27.00	12.68	23.00	22.22	14.17	14.33	13.00	12.67
As (ppm)	22.50	4.44	11.67	22.17	6.67	7.33	4.75	7.00
Co (ppm)	17.19	8.80	15.00	15.44	10.00	11.33	9.00	10.67
Zr/Fe	0.005	0.006	0.007	0.005	0.007	0.008	0.011	0.008
Zr/Rb	1.75	1.42	1.96	1.86	1.79	2.40	2.40	2.15
Cu/Zn	0.34	0.23	0.33	0.36	0.29	0.33	0.29	0.31

Unit V (80–35cm, OFD2): This unit can be divided into three sections according to the element content distribution (Figures 4, 5). As a whole, the SiO_2, Na_2O, Ba, Cr contents increase and the contents of Al_2O_3, Fe_2O_3, CaO, K_2O, MgO, Ti, Mn, P, S, Zr, Zn, Cu, Rb and Sr decrease significantly in this unit. Notable, the high content elements such as SiO_2, Na_2O, Ba, Cr are more abundant in OFD2-2 than OFD2-1 and OFD2-3 and the low-value elements in OFD2-2 are even scarcer (Table 2; Figures 4, 5). The average Zr/Fe, Zr/Rb ratios increase significantly and reach the maximum (0.011, 2.40) in OFD2-2. The average Cn/Zn ratio decrease and reach the minimum of the whole section in OFD2-2 with the values of 0.29 (Table 2; Figures 4, 5).

Unit VI (35–0 cm): The SiO_2, Ba, Cr contents drop sharply and the Al_2O_3, Fe_2O_3, K_2O, MgO, Ti, Mn, Zr, Rb, Zn, Cu contents in this unit appear high values again compared with those in Unit V (Figures 4, 5). The contents of Na_2O, CaO, Sr drop sharply to minimum in the surface layer while the contents of P, S increase dramatically to the maximum of the whole section. The Zr/Fe ratio decreases to the minimum and the average Cu/Zn ratio increases (Table 2; Figures 4, 5).

4.4 Results of principal component analysis

The element geochemistry is vertically consistent with stratigraphic change in the profile NYQ-B revealing distinct distribution patterns (Figures 4, 5). Principal component analysis (PCA) is used to extract the important information from a multivariate data table and to express this information as a set of few new variables called principal components (PC). The PCA of the element concentration data from the NYQ-B profile revealed that 84.06% of the sample variance is associated with the first two principal components (PC1 and PC2) and the first principal

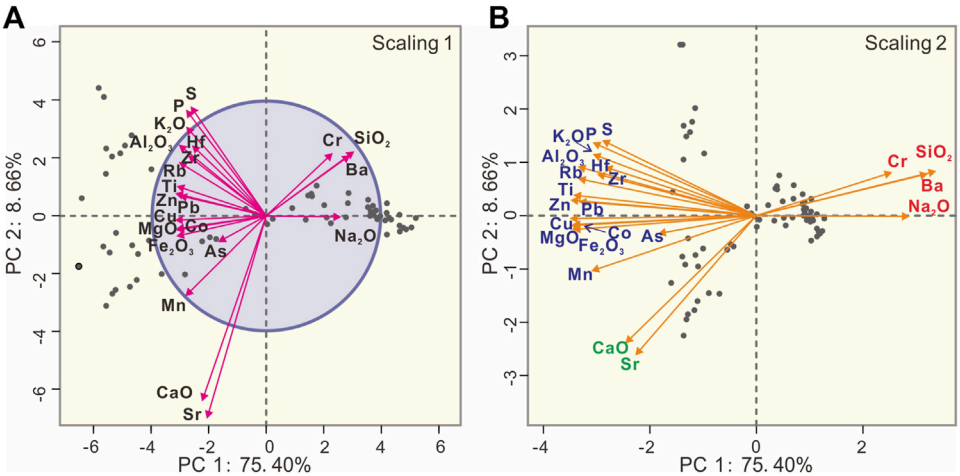

FIGURE 6
Principal component analysis of element concentration data of the paleo-oxbow lake fill at NYQ-B site within the Zoige Basin on the NE Tibetan Plateau. Elemental projections over the distance biplot using scaling 1 **(A)** and over the correlation biplot using scaling 2 **(B)** onto the first two principal components (PC1 and PC2).

component (PC1) account for 75.4% of the total variance (Figure 6). Therefore the PC 1 predominantly contribute toward the variability in the elemental dataset. The samples are plotted and elements are projected over the distance biplot (scaling 1) and the correlation biplot (scaling 2) (Figure 6). The correlation biplot reveals that elements distributed in sedimentary strata can be divided into three distinct element clusters (Figure 6B). A cluster comprising Ba, Cr, Na and SiO_2 is characterized by high positive scores of the PC1, slightly positive scores of the PC2 (Figure 6B), whose concentrations tend to increase in the most prominent sandy layers (Figures 4, 5). And another cluster with high negative PC1 scores, slightly positive or negative PC2 scores (Figure 6B), comprises Al_2O_3, Fe_2O_3, MgO, K_2O, Cu, Zn, Pb, Zr, Rb, Mn, P, S and other trace elements, showing decreasing concentrations in the sandy layers (Figures 4, 5). So we suggest that the PC 1 can be associated with the grain-size, which means the element distribution of the paleo-oxbow lake fill at NYQ-B site is controlled mainly by grain-size variation. A cluster comprising Sr, CaO is characterized by high negative PC1 scores and high negative PC2 scores (Figure 6B). In addition, the arrow lengths of the P, S, Sr and CaO in distance biplot are much longer than the radius of the circle of equilibrium contribution (Figure 6A), indicating that their contribution to the PC1 and PC2 are greater than the average contribution of other variables. PC2 (8.66% of sample variance) is presumably related to the effect of the element source. The highly negative scores of Sr and CaO are assumed to indicate source from authigenic carbonate (Chen et al., 1999b).

5 Discussion

5.1 Identification of oxbow lake evolution and extreme overbank flooding

Oxbow lakes form from the cut-off and sealing of previous meanders due to bank erosion and flooding within the Zoige Basin on the NE Tibetan Plateau (Li and Gao, 2019; Huang, 2021), and provide archives to reconstruct the paleo-channel evolution and the flooding history of the Yellow River during the Holocene. The elemental distribution in each sedimentary unit of the NYQ-B profile show obviously different characteristics (Figures 4, 5) and our PCA results prove that distribution pattern is controlled mainly by grain-size variation (Figure 6). Wolfe et al. (2006) report on a close correlation between flood events and high energy discharge marked by an increased influx of coarse grained detrital material into the river coupled with a relative decrease in the clay fraction. Significant correlations between turbidity and some trace elements were interpreted by Berner et al. (2012) due to the sorption of metals onto fine-grain size particles particles. So we suggest that chemical elements can be applied in defining the paleoflood deposits in the paleo-oxbow profile and have important tracing significance on studies about the regional channel evolution (Zhang et al., 2012). Meanwhile, the Zr/Rb and the Zr/Fe ratios provides a robust geochemical proxy for flood deposits across floodplain in this study (Fuller et al., 2018; Munoz et al., 2018). The element Zr is found principally in the resistant mineral zircon, tending to become concentrated in fine sand to coarse silt, while Rb and Fe is found in a range of minerals including clay minerals and concentrates in fine silt and clay, which means an increasing Zr/Rb and Zr/Fe ratio can be associated with an increase in grain size (Jones et al., 2012). Besides, the Cu/Zn ratio is used as a reference to judge the oxidation-reduction status of the sedimentary environment of the paleochannel (Fan et al., 2022). On the basis of the lithological, grain size, and compelling geochemical evidence presented, we propose that the development of the paleo-river channel NYQ-B including 6 phases: a fluvial environment, two oxbow lake environment and a steppe environment, interrupted by two episodes of overbank flooding.

Phase I: The dull yellowish orange medium sands can be identified at the bottom of the profile NYQ-B (Unit I-Riverbed deposits). The Unit I (215–340 cm) is dominated by coarse sand with some rust spots and inclined beddings (Figure 3) and characterized by the high contents of SiO_2 contained in sand-

sized quartz grains in local river systems (Figure 4), which can represent the riverbed deposits of the ancient Yellow River. It can be indicated that the ancient Yellow River flowed through the site before 3,240 ± 260 a (Xiao et al., 2022). This riverbed deposits of the ancient Yellow River below 330 cm is blue-gray and has a low value of Cu/Zn ratio, which indicates that it is a weakly reducing environment (Mei, 1988). It is speculated that the gleying process occurred because the lower part of the section was submerged by water for a long time due to the high groundwater level, which transformed the ferric iron into ferrous compound (Lu et al., 2012).

Phase II: The Unit II (215–200 cm, OLD-A) has a sharp contact with the Unit I and is composed of brown black clayey silt, with a hard texture and rich in organic matter. Such vertical changes in the sedimentary texture and structure indicate that the previous river channel was cut off and the abandoned river channel was filled up by suspended-load sediments on floodplains in an environment of slowly flowing to stagnant water (Toonen et al., 2012). It suggests that the fluvial sedimentary environment was replaced by the oxbow lake sedimentary environment. This is also proven by the results of the concentration of lithophilic elements (Al, Fe, K and Mg) and elements concentrate in fine silt and clay (Ti, Rb), which are highly correlated by according to our PCA results and indicate the abundant delivery of fine-grained detrital material into the paleo-oxbow lake (Sedláček et al., 2019; Antczak-Orlewska et al., 2021). We considered that the ancient Yellow River completed the nature cutoff (neck cutoff) at 3,240 ± 260 a, and this river channel was gradually abandoned and formed the paleo-oxbow lake (Xiao et al., 2022).

Phase III: The Unit III (200–170 cm, OFD1) has a sharp boundary with Unit II, which comprises yellowish orange sand with some rust spots and parallel or waving beddings. This stratigraphical structures is typical of overbank flood deposits. According to the grain size analysis, significantly higher proportions of sand occurred in Unit III. Sandy layers and low χ_{fd} values give evidence of the accumulation phase during flood events and represent typical overbank flood deposits (Figure 3). The high contents of SiO_2 reveals that the OFD1 unit is also dominated by the coarse sand-sized quartz grains (Galicki et al., 2018). It can be concluded that although the paleochannel (paleo-oxbow lake type) of the Yellow River has formed at 3,240 ± 260 a, extreme overbank flooding at 2,960 ± 0.24–2,870 ± 270 a accessed into the paleo-oxbow lake and resulted in high sedimentation rates (Wolfe et al., 2006; Xiao et al., 2022).

Phase IV: the grain size of the Unit IV (170–80 cm, OLD-B) became fine rapidly and the color changed from yellowish orange to brown, indicating the sedimentary environment is transformed to the oxbow lake environment again. Compared to the previous paleo-oxbow environment (Phase II), this layer is characterized by the obvious interbedding of the clay silt and fine sandy silt, a comparatively large fluctuation of element contents and the highly concentrated soluble elements (Ca, Sr). The high values of Sr and CaO in the lake sediments were caused by authigenic carbonate precipitation, suggesting a shrinking and progressively more saline lake as the climate gradually became drier (Chen et al., 2010). A generally drier climate and weaker vegetation coverage in the basin after 3000 BP was also indicated by the pollen record from the eastern margin of the Tibetan Plateau (Zhou et al., 2010). This implies that the intensity of the summer monsoon was weakening during this period (Wang et al., 2005; Hu et al., 2008).

Phase V: The Unit V (80–35 cm, OFD2) can be divided into three sublayers: the OFD2-1 and OFD2-3 comprises yellowish orange silty fine sand, while the OFD2-2 has a lighter color and a coarser grain size composed of grayish-white silty fine sand, and it could be resulted from three episodes of extreme overbank flooding with different magnitudes at 1840 ± 200–1700 ± 160 a. The OFD2 unit is also detected by the Zr/Fe, Zr/Rb ratios, which reach to the maximum value of the whole profile, due to the large amount of heavy mineral transported into the lake environment by high energy discharge during floods (Fuller et al., 2018; Munoz et al., 2018).

Phase VI: The Unit V merges gradually into Unit VI (35–0 cm, Modern soil) after 1,310 ± 50 a, a layer of typical subalpine meadow soil, which comprises grey clayey silt with abundant earthworm burrows and plant roots. The fine-grained sediment and the enrichment of Al, Fe, K, Mg, Ti, Rb indicate that pedogenesis processes occurred at the NYQ-B site (Jia et al., 2022). The high concentration of P and S in surface layer are presumed to indicate the influence of anthropogenic pollution (Akhtar et al., 2003).

5.2 The link between climate change and extreme overbank flooding

The general characteristics of climatic and environmental changes during Holocene can be reflected by the evolution phases of the paleo-oxbow lake fill at NYQ-B site within the Zoige Basin on the NE Tibetan Plateau. Especially, the climatic background and inducing factors of extreme overbank flooding recorded by flood units are inferred in this study. Previous studies have proposed that extraordinary floods often result from an abrupt change of climate and climatic deterioration (Guo et al., 2000; Huang et al., 2007). The OFDs in the NYQ-B profile are easily differentiated from oxbow lake deposits in terms of the significantly higher proportions of sand, enriched content of SiO_2 (even above 80%) and the increase in silicate-bound elements (Na, Ba and Cr). It is confirmed that two phases of extreme overbank flooding prevailed within the Zoige Basin between 2,960 ± 240–2,870 ± 270 a and 1840 ± 200–1700 ± 160 a, respectively. And we infer these high intensity of floods on the NE Tibetan Plateau result from increase in extreme rainstorms during the late Holocene climatic deterioration and are considered as a response of the regional fluvial system to high climatic variability and instability.

The first extreme flooding episode (2,960 ± 240–2,870 ± 270 a) recorded by OFD1 in the NYQ-B profile is coincide with the climatic deterioration during mid-Holocene climatic optimum to the late Holocene (Peng et al., 2005; Huang et al., 2009). Because the Megathermal fell into decline and global climate entered a drastic fluctuation period around 3,000 a BP, the climate became highly variable and instabilized in the transition from the dominance of the maritime monsoon to continental monsoon (Xiao et al., 2004; Wang et al., 2005; Hu et al., 2008). Studies on the relationships between modern floods and the monsoonal climate have indicated that extraordinary flood events often resulted from infrequent rainstorms in connection with unusual atmospheric circulation

patterns (Knox, 2000; Huang et al., 2007; Guo et al., 2016; Huang, 2021). Therefore, we infer that an abrupt climatic deterioration with extreme climate variability around 3,000 a BP at the end of the mid-Holocene Climate Optimum caused a series of disasters in different areas in China's monsoonal regions, including extraordinary floods due to increased precipitation in the source region of Yellow River (Kale et al., 2000; Grossman, 2001; Bohorquez et al., 2013; Lillios et al., 2016). Previous researches of the middle Yellow River also provide evidence that some extreme flooding events occurred at the Weihe River, Jinghe River and Beiluo River between 3,200 a BP to 2,800 a BP (Huang et al., 2012; Wan et al., 2015; Li et al., 2019). Historical documents show that the collapses of the Shang Dynasty (1,600–1046 BCE) were attributed to disastrous events including extreme floods, droughts, famines and desiccation of the Yellow River and its tributaries during this period (Huang et al., 2009).

Moreover, severe droughts resulting from shortage of rainfall and extraordinary floods resulting from rainstorms were two parts of the extreme climate variability during climatic events (Huang et al., 2007; Huang et al., 2010; Huang et al., 2013; Guo et al., 2015; Guo et al., 2016; Li et al., 2019; Li et al., 2021). Although great floods occurred as a result of extreme rainstorms in the Zoige Basin, deposits from Qinghai Lake and its surrounding aeolian deposits have documented decreasing temperature and increasing aridity after ca. 3,100 a BP (Shen et al., 2005; Li et al., 2017). Meanwhile, the colder and drier regime around 3,000 a BP is also identified in Nile Delta and severe centennial-scale droughts may have affected civilizations in northern Africa, southwestern Asia and mid-continental North America Middle (Bernhardt et al., 2012). It was suggested that the precipitation variability might be resulted from the complex feedback process between various high- and low-latitude competing driving forces, implying a large-scale climatic teleconnection across the Northern Hemisphere (Li et al., 2017).

The second episode of extreme flooding events recorded by OFD2 in the NYQ-B profile occurred at 1840 ± 200–1700 ± 160 a correlated with cooling and desiccation periods during the Dark Age Cold Period (DACP) (1800–1,100 a; Patterson et al., 2010). This flood episode on the NE Tibetan Plateau shows good agreement in terms of the low values of $\delta^{18}O$ from ice-cores of the GRIP which indicates that the climate cooled significantly during this period (Dansgaard et al., 1993). Some high resolution climatic proxies and precise dating from stalagmites provide information on weakening of monsoon activities at that time (Wang et al., 2005; Hu et al., 2008). The increased flood activities during the Dark Age Cold Period are also correspond to the reconstructed paleoflood events in the middle Yangtze River (Guo et al., 2016) and reported by other documentary and sedimentary archives from the Austrian Pre-Alps (Swierczynski et al., 2012) and the western Europe (Pears et al., 2020). This flood phase generally corresponds to the period of the Eastern Han Dynasty (CE 25–220) in Chinese history and the floods, droughts, large-scale famine and frequent change of dynasties are recorded in ancient Chinese documents (Zheng et al., 1999).

Overall, two episodes of increased flood activities on the NE Tibetan Plateau occurred at global deterioration periods with highly climate instability. Great floods occurred as a result of extreme rainstorms caused by special atmospheric circulation patterns that determine the location of storm tracks and air mass boundaries, resulting in excessive runoff and flooding (Knox, 2000). In particular, glacier advanced and the glacial meltwater supply decreased on the NE Tibetan Plateau due to the colder and drier climate from 3,100 to 2,600 a and 1800–1,300 a (Lehmkuhl, 1997; Mischke and Zhang, 2010), which means the contribution of ice and snow melting to the two episodes of overbank flooding may be relatively weak. However, when climate departed from its normal condition during late Holocene, the weak summer monsoon and strong Western Pacific Subtropical High (WPSH) occur in the Yellow River catchment, and the warm-humid air masses brought by EASM and ISM meets the northern cold airflow brought by northwestern continental monsoon (Ma and Xu, 1982). Therefore, we consider that large-magnitude floods on the NE Tibetan Plateau is caused by long-duration rainstorms due to the quasistationary front hovers above the upper Yellow River catchment (Guo et al., 2016). Similar historical and modern flooding events within the Zoige Basin due to the extreme precipitation have been reported by previous studies (Wang, 2012). Therefore, we believe that the strong rainfall caused by abnormal atmospheric circulation during the period of climate transition/abrupt change may be the main triggering factor of these two episodes of extreme overbank flooding (Xiao et al., 2022).

6 Conclusion

The sedimentary section of the paleo-oxbow lake fill at NYQ-B site was discovered after the observation of aerial photographs and maps within the Zoige Basin on the NE Tibetan Plateau. The multi-proxy approach especially geochemical proxy to the interpretation of the NYQ-B paleo-oxbow sedimentary infill enables us to reconstruct the evolution of river channel, local sedimentation processes and extreme flooding history linked to global climate changes. The following conclusions are drawn:

1. The sediment of the paleo-oxbow lake fill at NYQ-B site contained the paleoenvironmental record during middle to late Holocene. The paleo-oxbow lake fill was occupied by the ancient Yellow River during 4,170 ± 490–3,240 ± 260 a. After the neck cutoff of the Yellow River and abandonment of the channel, the shallow oxbow lake appeared at 3,240 ± 260 a, interrupted by two episodes of extraordinary overbank flooding, changed to a steppe environment at 1,310 ± 50 a and continue to the present day.
2. Geochemical characteristics can be used as the robust proxy to identify the flood deposits accurately in the Holocene stratum of the fluvial plain on the NE Tibetan Plateau. The elemental distribution in each sedimentary unit of the profile NYQ-B show obviously different characteristics with a certain relationship with grain-size variation. Layers of overbank flood deposits are characterized by the high contents of SiO_2, Na_2O, Ba, low contents of Al_2O_3, Fe_2O_3, MgO, K_2O, Ti, Rb and high values of Zr/Fe, Zr/Rb ratios.
3. Two episodes of extraordinary overbank flooding in the upper Yellow River occurred during 2,960 ± 240–2,870 ± 270 a and 1840 ± 200–1700 ± 160 a, which are in good agreement with the transition periods from the mid-Holocene climatic optimum to the late Holocene and the Dark Age Cold

Period (DACP). Abnormal atmospheric circulation and strong rainfall during the period of climate transition and abrupt change triggered extreme flooding on the NE Tibetan Plateau, which is helpful in understanding the regional response of hydroclimatic system to climatic variations in source region of the largest rivers of Asia.

Data availability statement

The original contributions presented in the study are included in the article/Supplementary Material, further inquiries can be directed to the corresponding author.

Author contributions

ShW: analyzing and synthesizing study data, writing the initial draft; NW: Management and coordination responsibility for the research activity planning and execution; YuZ: Formulation of overarching research goals and design of methodology; CH: Data collection and software programming; YaZ: Conducting the investigation process; QX: Performing the OSL dating experiments; DC: Performing the geochemical experiments; HW: Performing the experiments of Magnetic susceptibility; YM and XH: Performing the experiments of Grain-size distribution; SiW: Reviewing and editing the manuscript.

Funding

This work was supported by the grants from the National Science Foundation of China (42277449, 4197116), the Chinese Postdoctoral Science Foundation (2022M722570), the Second Tibetan Plateau Scientific Expedition and Research Program (2019QZKK0903), Strategic Priority Research Program of the Chinese Academy of Sciences (XDA20060201), and the Open Foundation of The State Key Laboratory of Loess and Quaternary Geology (SKLLQG2107).

Conflict of interest

The authors declare that the research was conducted in the absence of any commercial or financial relationships that could be construed as a potential conflict of interest.

Publisher's note

All claims expressed in this article are solely those of the authors and do not necessarily represent those of their affiliated organizations, or those of the publisher, the editors and the reviewers. Any product that may be evaluated in this article, or claim that may be made by its manufacturer, is not guaranteed or endorsed by the publisher.

References

Akhtar, M., Richards, B., Medrano, P., deGroot, M., and Steenhuis, T. (2003). Dissolved phosphorus from undisturbed soil cores. *Soil Sci. Soc. Am. J.* 67, 458–470. doi:10.2136/sssaj2003.0458

An, Z., Colman, S., Zhou, W., Li, X., Brown, E., Jull, A., et al. (2012). Interplay between the westerlies and asian monsoon recorded in lake Qinghai sediments since 32 ka. *Sci. Rep.* 2, 619. doi:10.1038/srep00619

Antczak-Orlewska, O., Okupny, D., Pawłowski, D., Kotrys, B., Krąpiec, M., Luoto, T. P., et al. (2021). The environmental history of the oxbow in the Luciąża River valley – study on the specific microclimate during Allerød and Younger Dryas in central Poland. *Quat. Int.* 644-645, 178–195. doi:10.1016/j.quaint.2021.08.011

Arnaud, F., Poulenard, J., Giguet-Covex, C., Wilhelm, B., Révillon, S., Jenny, J.-P., et al. (2016). Erosion under climate and human pressures: An alpine lake sediment perspective. *Quat. Sci. Rev.* 152, 1–18. doi:10.1016/j.quascirev.2016.09.018

Bábek, O., Faměra, M., Hilscherová, K., Kalvoda, J., Dobrovolný, P., Sedláček, J., et al. (2011). Geochemical traces of flood layers in the fluvial sedimentary archive; implications for contamination history analyses. *Catena* 87, 281–290. doi:10.1016/j.catena.2011.06.014

Baker, V. (1987). Paleoflood hydrology and extraordinary flood events. *J. Hydrology* 96, 79–99. doi:10.1016/0022-1694(87)90145-4

Berner, Z., Bleeck-Schmidt, S., Stüben, D., Neumann, T., Fuchs, M., and Lehmann, M. (2012). Floodplain deposits: A geochemical archive of flood history – a case study on the river rhine, Germany. *Appl. Geochem.* 27, 543–561. doi:10.1016/j.apgeochem.2011.12.007

Bernhardt, C., Horton, B., and Stanley, J. (2012). Nile Delta vegetation response to Holocene climate variability. *Geology* 40, 615–618. doi:10.1130/g33012.1

Bohorquez, P., García-García, F., Pérez-Valera, F., and Martínez-Sánchez, C. (2013). Unsteady two-dimensional paleohydraulic reconstruction of extreme floods over the last 4000 yr in Segura River, southeast Spain. *J. hydrology* 477, 229–239. doi:10.1016/j.jhydrol.2012.11.031

Borcard, D., Gillet, F., and Legendre, P. (2018). "Unconstrained ordination," in *Numerical ecology with R* (Springer), 151–201.

Brown, E. (2011). Lake Malawi's response to "megadrought" terminations: Sedimentary records of flooding, weathering and erosion. *Palaeogeogr. Palaeoclimatol. Palaeoecol.* 303, 120–125. doi:10.1016/j.palaeo.2010.01.038

Chen, F., Bloemendal, J., Zhang, P., and Liu, G. (1999b). An 800 ky proxy record of climate from lake sediments of the Zoige Basin, eastern Tibetan Plateau. *Palaeogeogr. Palaeoclimatol. Palaeoecol.* 151, 307–320. doi:10.1016/s0031-0182(99)00032-2

Chen, J., An, Z., and Head, J. (1999a). Variation of Rb/Sr ratios in the loess-paleosol sequences of central China during the last 130,000 Years and their implications for monsoon paleoclimatology. *Quat. Res.* 51, 215–219. doi:10.1006/qres.1999.2038

Chen, H., Song, S., Lee, T., Löwemark, L., Chi, Z., Wang, Y., et al. (2010). A multiproxy lake record from Inner Mongolia displays a late Holocene teleconnection between Central Asian and North Atlantic climates. *Quat. Int.* 227, 170–182. doi:10.1016/j.quaint.2010.03.005

Chen, F., Wu, D., Chen, J., Zhou, A., Yu, J., Shen, J., et al. (2016). Holocene moisture and East Asian summer monsoon evolution in the northeastern Tibetan plateau recorded by lake Qinghai and its environs: A review of conflicting proxies. *Quat. Sci. Rev.* 154, 111–129. doi:10.1016/j.quascirev.2016.10.021

Dansgaard, W., Johnsen, S., Clausen, H., Dahl-Jensen, D., Gundestrup, N., Hammer, C., et al. (1993). Evidence for general instability of past climate from a 250-kyr ice-core record. *nature* 364, 218–220. doi:10.1038/364218a0

Fan, Q., Xia, G., Li, G., and Yi, H. (2022). Analytical methods and research progress of redox conditions in the paleo-ocean. *Acta Sedimentol. Sin.* 40, 1151–1171. (In Chinese with English abstract). doi:10.14027/j.issn.1000-0550.2021.023

Francke, A., Holtvoeth, J., Codilean, A., Lacey, J., Bayon, G., and Dosseto, A. (2020). Geochemical methods to infer landscape response to quaternary climate change and land use in depositional archives: A review. *Earth-Science Rev.* 207, 103218. doi:10.1016/j.earscirev.2020.103218

Fritz, M., Unkel, I., Lenz, J., Gajewski, K., Frenzel, P., Paquette, N., et al. (2018). Regional environmental change versus local signal preservation in Holocene thermokarst lake sediments: A case study from herschel island, yukon (Canada). *J. Paleolimnol.* 60, 77–96. doi:10.1007/s10933-018-0025-0

Fuller, I., Macklin, M., Toonen, W. H., and Holt, K. (2018). Storm-generated Holocene and historical floods in the manawatu river, New Zealand. *Geomorphology* 310, 102–124. doi:10.1016/j.geomorph.2018.03.010

Fuller, I., Macklin, M., Toonen, W., Turner, J., and Norton, K. (2019). A 2000 year record of palaeofloods in a volcanically-reset catchment: Whanganui River, New Zealand. *Glob. Planet. Change* 181, 102981. doi:10.1016/j.gloplacha.2019.102981

Galicki, S., Bujenovic, M., Woehnker, T., Galtney, J., and Galicki, T. (2018). Mid-late Holocene anthropogenic and natural variations in geochemistry and sedimentation in the yazoo basin: Clark lake, sharkey county, Mississippi. *Phys. Geogr.* 40, 209–226. doi:10.1080/02723646.2018.1516395

Goldberg, K., and Humayun, M. (2010). The applicability of the chemical index of alteration as a paleoclimatic indicator: An example from the permian of the paraná basin, Brazil. *Braz. Palaeogeogr. Palaeoclimatol. Palaeoecol.* 293, 175–183. doi:10.1016/j.palaeo.2010.05.015

Grossman, M. (2001). Large floods and climatic change during the Holocene on the Ara river, central Japan. *Geomorphology* 39, 21–37. doi:10.1016/s0169-555x(01)00049-6

Gu, H., Yu, Z., Yang, C., and Ju, Q. (2018). Projected changes in hydrological extremes in the Yangtze River basin with an ensemble of regional climate simulations. *Water* 10, 1279. doi:10.3390/w10091279

Guo, Z., Petit-Maire, N., and Kröpelin, S. (2000). Holocene non-orbital climatic events in present-day arid areas of northern Africa and China. *Glob. Planet. Change* 26, 97–103. doi:10.1016/s0921-8181(00)00037-0

Guo, Y., Huang, C., Pang, J., Zha, X., Zhou, Y., Wang, L., et al. (2015). Investigating extreme flood response to Holocene palaeoclimate in the Chinese monsoonal zone: A palaeoflood case study from the hanjiang river. *Geomorphology* 238, 187–197. doi:10.1016/j.geomorph.2015.03.014

Guo, Y., Huang, C., Zhou, Y., Pang, J., Zha, X., Zhou, L., et al. (2016). Extraordinary flood events and the response to monsoonal climatic change during the last 3000 years along the middle Yangtze River valley, China. *Palaeogeogr. Palaeoclimatol. Palaeoecol.* 462, 70–84. doi:10.1016/j.palaeo.2016.09.005

Guo, X., Gao, P., and Li, Z. (2021). Morphological characteristics and changes of two meandering rivers in the Qinghai-Tibet Plateau, China. *Geomorphology* 379, 107626. doi:10.1016/j.geomorph.2021.107626

Hasberg, A., Bijaksana, S., Held, P., Just, J., Melles, M., Morlock, M., et al. (2019). Modern sedimentation processes in Lake Towuti, Indonesia, revealed by the composition of surface sediments. *Sedimentology* 66, 675–698. doi:10.1111/sed.12503

Hu, C., Henderson, G., Huang, J., Xie, S., Sun, Y., and Johnson, K. (2008). Quantification of Holocene Asian monsoon rainfall from spatially separated cave records. *Earth Planet. Sci. Lett.* 266, 221–232. doi:10.1016/j.epsl.2007.10.015

Hu, G., Yu, L., Dong, Z., Lu, J., Li, J., Wang, Y., et al. (2018). Holocene aeolian activity in the Zoige Basin, northeastern Tibetan plateau, China. *Catena* 160, 321–328. doi:10.1016/j.catena.2017.10.005

Huang, C. (2021). Palaeoflood deposits in the Zoige Basin and the enlightening on the formation of the Yellow River drainage system on the Tibetan plateau. *Acta Geogr. Sin.* 76, 612–625. (In Chinese with English abstract). doi:10.11821/dlxb202103009

Huang, C., Pang, J., Zha, X., Su, H., Jia, Y., and Zhu, Y. (2007). Impact of monsoonal climatic change on Holocene overbank flooding along Sushui River, middle reach of the Yellow River, China. *Quat. Sci. Rev.* 26, 2247–2264. doi:10.1016/j.quascirev.2007.06.006

Huang, C., Pang, J., Su, H., Li, S., and Ge, B. (2009). Holocene environmental change inferred from the loess–palaeosol sequences adjacent to the floodplain of the Yellow River, China. *Quat. Sci. Rev.* 28, 2633–2646. doi:10.1016/j.quascirev.2009.05.024

Huang, C., Pang, J., Zha, X., Zhou, Y., Su, H., and Li, Y. (2010). Extraordinary floods of 4100– 4000 a BP recorded at the late neolithic ruins in the Jinghe River gorges, middle reach of the Yellow River, China. *Palaeogeogr. Palaeoclimatol. Palaeoecol.* 289, 1–9. doi:10.1016/j.palaeo.2010.02.003

Huang, C., Pang, J., Zha, X., Su, H., and Jia, Y. (2011a). Extraordinary floods related to the climatic event at 4200 a BP on the Qishuihe River, middle reaches of the Yellow River, China. *Quat. Sci. Rev.* 30, 460–468. doi:10.1016/j.quascirev.2010.12.007

Huang, C., Pang, J., Zha, X., Zhou, Y., Su, H., Wan, H., et al. (2011b). Sedimentary records of extraordinary floods at the ending of the mid-Holocene climatic optimum along the Upper Weihe River, China. *Holocene* 22, 675–686. doi:10.1177/0959683611409781

Huang, C., Pang, J., Zha, X., Zhou, Y., Su, H., Zhang, Y., et al. (2012). Holocene palaeoflood events recorded by slackwater deposits along the lower Jinghe River valley, middle Yellow River basin, China. *J. Quat. Sci.* 27, 485–493. doi:10.1002/jqs.2536

Huang, C., Pang, J., Zha, X., Zhou, Y., Yin, S., Su, H., et al. (2013). Extraordinary hydro-climatic events during the period AD 200– 300 recorded by slackwater deposits in the upper Hanjiang River valley, China. *Palaeogeogr. Palaeoclimatol. Palaeoecol.* 374, 274–283. doi:10.1016/j.palaeo.2013.02.001

Jia, Y., Zhang, Y., Huang, C., Wang, N., Qiu, H., Wang, H., et al. (2022). Weathering and pedogenesis of the late Pleistocene and Holocene aeolian loess-paleosol sections in the Yellow River source area, NE Tibetan Plateau. *Palaeogeogr. Palaeoclimatol. Palaeoecol.* 208, 111065. doi:10.1016/j.palaeo.2022.111065

Jones, A., Macklin, M., and Brewer, P. (2012). A geochemical record of flooding on the upper River Severn, UK, during the last 3750years. *Geomorphology* 179, 89–105. doi:10.1016/j.geomorph.2012.08.003

Kale, V., Singhvi, A., Mishra, P., and Banerjee, D. (2000). Sedimentary records and luminescence chronology of late Holocene palaeofloods in the luni river, thar desert, northwest India. *Catena* 40, 337–358. doi:10.1016/s0341-8162(00)00091-6

Knox, J. (2000). Sensitivity of modern and Holocene floods to climate change. *Quat. Sci. Rev.* 19, 439–457. doi:10.1016/s0277-3791(99)00074-8

Kołaczek, P., Gałka, M., Apolinarska, K., Gębica, P., Superson, S., Michno, A., et al. (2017). Lost in dating – problems with the absolute chronologies and sedimentation rates of Late Glacial and Early Holocene oxbow lake deposits in Central Europe. *Quat. Geochronol.* 41, 187–201. doi:10.1016/j.quageo.2017.05.002

Legendre, P., and Gallagher, E. (2001). Ecologically meaningful transformations for ordination of species data. *Oecologia* 129, 271–280. doi:10.1007/s004420100716

Lehmkuhl, F. (1997). Late Pleistocene, late-glacial and Holocene glacier advances on the Tibetan plateau. *Quat. Int.* 38, 77–83. doi:10.1016/s1040-6182(96)00025-0

Li, J., Dodson, J., Yan, H., Cheng, B., Zhang, X., Xu, Q., et al. (2017). Quantitative precipitation estimates for the northeastern Qinghai-Tibetan Plateau over the last 18,000 years. *J. Geophys. Res. Atmos.* 122, 5132–5143. doi:10.1002/2016jd026333

Li, Y., Huang, C., Ngo, H., Pang, J., Zha, X., Liu, T., et al. (2019). *In situ* reconstruction of long-term extreme flooding magnitudes and frequencies based on geological archives. *Sci. total Environ.* 670, 8–17. doi:10.1016/j.scitotenv.2019.03.066

Li, Y., Huang, C., Ngo, H., Yin, S., Dong, Z., Zhang, Y., et al. (2021). Analysis of event stratigraphy and hydrological reconstruction of low-frequency flooding: A case study on the fenhe river, China. *J. Hydrology* 603, 127083. doi:10.1016/j.jhydrol.2021.127083

Li, Z., and Gao, P. (2019). Channel adjustment after artificial neck cutoffs in a meandering river of the Zoige basin within the Qinghai-Tibet Plateau, China. *Catena* 172, 255–265. doi:10.1016/j.catena.2018.08.042

Lillios, K., Blanco-González, A., Drake, B., and López-Sáez, J. (2016). Mid-late Holocene climate, demography, and cultural dynamics in iberia: A multi-proxy approach. *Quat. Sci. Rev.* 135, 138–153. doi:10.1016/j.quascirev.2016.01.011

Liu, Q., Torrent, J., Maher, B., Yu, Y., Deng, C., Zhu, R., et al. (2005). Quantifying grain size distribution of pedogenic magnetic particles in Chinese loess and its significance for pedogenesis. *J. Geophys. Res. Solid Earth* 110, B11102. doi:10.1029/2005jb003726

Lu, S., Zhu, L., and Yu, J. (2012). Mineral magnetic properties of Chinese paddy soils and its pedogenic implications. *Catena* 93, 9–17. doi:10.1016/j.catena.2012.01.002

Lutz, A., Immerzeel, W., Kraaijenbrink, P., Shrestha, A., and Bierkens, M. (2016). Climate change impacts on the upper indus hydrology: Sources, shifts and extremes. *PLoS One* 11, e0165630. doi:10.1371/journal.pone.0165630

Ma, J., and Xu, G. (1982). Extreme flood of the upper Yellow River in the fall of 1981. *Meteorol. Mon.* 8, 7–9. (In Chinese). doi:10.7519/j.issn.1000-0526.1982.04.002

Mei, S. (1988). Application of rock chemistry in the study of presinian sedimentary environment and the source of uranium mineralization in Hunan province. *Hunan Geol.* 7, 25–49. (In Chinese with English abstract).

Mischke, S., and Zhang, C. (2010). Holocene cold events on the Tibetan Plateau. *Glob. Planet. Change* 72, 155–163. doi:10.1016/j.gloplacha.2010.02.001

Munoz, S., Giosan, L., Therrell, M., Remo, J., Shen, Z., Sullivan, R., et al. (2018). Climatic control of Mississippi River flood hazard amplified by river engineering. *Nature* 556, 95–98. doi:10.1038/nature26145

Patterson, W., Dietrich, K., Holmden, C., and Andrews, J. (2010). Two millennia of North Atlantic seasonality and implications for Norse colonies. *Proc. Natl. Acad. Sci.* 107, 5306–5310. doi:10.1073/pnas.0902522107

Pawłowski, D., Kowalewski, G., Milecka, K., Płóciennik, M., Woszczyk, M., Zieliński, T., et al. (2015). A reconstruction of the palaeohydrological conditions of a flood-plain: A multi-proxy study from the grabia river valley mire, central Poland. *Boreas* 44, 543–562. doi:10.1111/bor.12115

Pears, B., Brown, A., Toms, P., Wood, J., Sanderson, D., and Jones, R. (2020). A sub-centennial-scale optically stimulated luminescence chronostratigraphy and late Holocene flood history from a temperate river confluence. *Geology* 48, 819–825. doi:10.1130/g47079.1

Peng, Y., Xiao, J., Nakamura, T., Liu, B., and Inouchi, Y. (2005). Holocene East Asian monsoonal precipitation pattern revealed by grain-size distribution of core sediments of Daihai Lake in Inner Mongolia of north-central China. *Earth Planet. Sci. Lett.* 233, 467–479. doi:10.1016/j.epsl.2005.02.022

Petr, L., Sádlo, J., Žáčková, P., Lisá, L., Novák, J., Rohovec, J., et al. (2013). Late-glacial and Holocene environmental history of an oxbow wetland in the polabí lowland (river elbe, Czech republic); a context-dependent interpretation of a multi-proxy analysis. *Folia Geobot.* 49, 137–162. doi:10.1007/s12224-013-9171-3

Ringnér, M. (2008). What is principal component analysis? *Nat. Biotechnol.* 26, 303–304. doi:10.1038/nbt0308-303

Sedláček, J., Kapustová, V., Šimíček, D., Bábek, O., and Sekanina, M. (2019). Initial stages and evolution of recently abandoned meanders revealed by multi-proxy methods in the Odra River (Czech Republic). *Geomorphology* 333, 16–29. doi:10.1016/j.geomorph.2019.02.027

Shehata Ahmed Hussein, A. (2016). *The role of mineral composition, rock permeability, and connate-water composition on the performance of low-salinity waterflooding in sandstone reservoirs*. Doctoral dissertation. College Station, TX: Department of Petroleum Engineering, Texas A&M University, 29–32.

Shen, J., Liu, X., Wang, S., and Matsumoto, R. (2005). Palaeoclimatic changes in the Qinghai Lake area during the last 18,000 years. *Quat. Int.* 136, 131–140. doi:10.1016/j.quaint.2004.11.014

Swierczynski, T., Brauer, A., Lauterbach, S., Martín-Puertas, C., Dulski, P., von Grafenstein, U., et al. (2012). A 1600 yr seasonally resolved record of decadal-scale flood variability from the Austrian Pre-Alps. *Geology* 40, 1047–1050. doi:10.1130/g33493.1

Ter Braak, C. (1983). Principal components biplots and alpha and beta diversity. *Ecology* 64, 454–462. doi:10.2307/1939964

Toonen, W., Kleinhans, M., and Cohen, K. (2012). Sedimentary architecture of abandoned channel fills. *Earth Surf. Process. Landforms* 37, 459–472. doi:10.1002/esp.3189

Toonen, W., Munoz, S., Cohen, K., and Macklin, M. (2020). "High-resolution sedimentary paleoflood records in alluvial river environments: A review of recent methodological advances and application to flood hazard assessment," in *Palaeohydrology* (Springer), 213–228.

Vogel, H., Russell, J., Cahyarini, S., Bijaksana, S., Wattrus, N., Rethemeyer, J., et al. (2015). Depositional modes and lake-level variability at Lake Towuti, Indonesia, during the past ~29 kyr BP. *J. Paleolimnol.* 54, 359–377. doi:10.1007/s10933-015-9857-z

Wan, H., Huang, C., and Pang, J. (2015). Major elements in the Holocene loess-paleosol sequence in the upper reaches of the Weihe River valley, China. *J. Arid Land* 8, 197–206. doi:10.1007/s40333-015-0020-5

Wang, Y., Cheng, H., Edwards, R., He, Y., Kong, X., An, Z., et al. (2005). The Holocene asian monsoon: Links to solar changes and north atlantic climate. *Science* 308, 854–857. doi:10.1126/science.1106296

Wang, J., Liang, Z., Wang, D., Liu, T., and Yang, J. (2016). Impact of climate change on hydrologic extremes in the upper basin of the Yellow River basin of China. *Adv. Meteorology* 2016, 1–13. doi:10.1155/2016/1404290

Wang, D., Li, Z., Li, Z., Pan, B., Tian, S., and Nie, X. (2020). Environmental gradient relative to oxbow lake-meandering river connectivity in Zoige Basin of the Tibetan Plateau. *Ecol. Eng.* 156, 105983. doi:10.1016/j.ecoleng.2020.105983

Wang, S., and Xue, B. (1997). Environmental evolution of zoigê basin since 900 ka B.P. And comparison study with loess plateau. *Sci. China Ser. D-Earth Sci.* 26, 329–336. (in Chinese). doi:10.1007/bf02877543

Wang, Z. (2012). Estimation of PMF for large-sized hydropower stations at the upper reach of longyangxia hydropower station on the Yellow River. *Northwest Hydropower* 130, 1–6. (In Chinese with English abstract). doi:10.3969/j.issn.1006-2610.2012.01.001

Wennrich, V., Minyuk, P., Borkhodoev, V., Francke, A., Ritter, B., Nowaczyk, N., et al. (2014). Pliocene to Pleistocene climate and environmental history of Lake El'gygytgyn, Far East Russian Arctic, based on high-resolution inorganic geochemistry data. *Clim. Past* 10, 1381–1399. doi:10.5194/cp-10-1381-2014

Wilhelm, B., Ballesteros Cánovas, J., Macdonald, N., Toonen, W., Baker, V., Barriendos, M., et al. (2018). Interpreting historical, botanical, and geological evidence to aid preparations for future floods. *Wiley Interdiscip. Rev. Water* 6, e1318. doi:10.1002/wat2.1318

Wolfe, B., Hall, R., Last, W., Edwards, T., English, M., Karst-Riddoch, T., et al. (2006). Reconstruction of multi-century flood histories from oxbow lake sediments, Peace-Athabasca Delta, Canada. *Hydrol. Process.* 20, 4131–4153. doi:10.1002/hyp.6423

Woolway, R., and Merchant, C. (2019). Worldwide alteration of lake mixing regimes in response to climate change. *Nat. Geosci.* 12, 271–276. doi:10.1038/s41561-019-0322-x

Wu, R. (1993). Magnetic susceptibility (χ) and frequency dependent susceptibility (χ_{fd}) of lake sediments and their paleoclimatic implication. *J. Lake Sci.* 5, 128–135. (In Chinese with English abstract). doi:10.18307/1993.0204

Xiao, J., Xu, Q., Nakamura, T., Yang, X., Liang, W., and Inouchi, Y. (2004). Holocene vegetation variation in the daihai lake region of north-central China: A direct indication of the asian monsoon climatic history. *Quat. Sci. Rev.* 23, 1669–1679. doi:10.1016/j.quascirev.2004.01.005

Xiao, Q., Zhang, Y., Wang, N., Huang, C., Qiu, H., Zhu, Y., et al. (2022). Paleochannel of the Yellow River within the Zoige Basin and its environmental significance on the NE Tibetan plateau. *Sci. Total Environ.* 853, 158242. doi:10.1016/j.scitotenv.2022.158242

Yang, H., Zhao, Y., Cui, Q., Ren, W., and Li, Q. (2020). Paleoclimatic indication of X-ray fluorescence core-scanned Rb/Sr ratios: A case study in the Zoige Basin in the eastern Tibetan plateau. *Sci. China Earth Sci.* 64, 80–95. doi:10.1007/s11430-020-9667-7

Zhang, Y., Huang, C., Pang, J., Zha, X., Zhou, Y., Zhou, Z., et al. (2012). Geochemical characteristics of the Holocene flooding slackwater deposits in the lower reaches of the Jinghe river. *Acta Sedimentol. Sin.* 30, 900–908. (In Chinese with English abstract). doi:10.14027/j.cnki.cjxb.2012.05.020

Zhang, G., Yao, T., Xie, H., Yang, K., Zhu, L., Shum, C. K., et al. (2020). Response of Tibetan Plateau lakes to climate change: Trends, patterns, and mechanisms. *Earth-Science Rev.* 208, 103269. doi:10.1016/j.earscirev.2020.103269

Zheng, J., Ge, Q., and Zhang, P. (1999). Abrupt climatic change: Evidence and implication. *Adv. Earth Sci.* 14, 76–81. (In Chinese with English abstract). doi:10.3321/j.issn:1001-8166.1999.02.013

Zhou, L., Oldfield, F., Wintle, A., Robinson, S., and Wang, J. (1990). Partly pedogenic origin of magnetic variations in Chinese loess. *Nature* 346, 737–739. doi:10.1038/346737a0

Zhou, W., Yu, S., Burr, G., Kukla, G., Jull, A., Xian, F., et al. (2010). Postglacial changes in the asian summer monsoon system: A pollen record from the eastern margin of the Tibetan plateau. *Boreas* 39, 528–539. doi:10.1111/j.1502-3885.2010.00150.x

Zhou, W., Liu, T., Wang, H., An, Z., Cheng, P., Zhu, Y., et al. (2016). Geological record of meltwater events at Qinghai Lake, China from the past 40 ka. *Quat. Sci. Rev.* 149, 279–287. doi:10.1016/j.quascirev.2016.08.005

Zhou, X., Xu, M., Wang, Z., Yu, B., and Shao, X. (2019). Responses of macroinvertebrate assemblages to environmental variations in the river-oxbow lake system of the Zoige wetland (Bai River, Qinghai-Tibet Plateau). *Sci. Total Environ.* 659, 150–160. doi:10.1016/j.scitotenv.2018.12.310